

Article

Band-Gap Properties of Finite Locally Resonant Beam Suspended Periodically with Two-Degree-of-Freedom Force Type Resonators

Hangyuan Lv ^{1,2,*} , Shangjie Li ¹, Xianzhen Huang ^{1,2} and Zhongliang Yu ³

¹ School of Mechanical Engineering and Automation, Northeastern University, Shenyang 110819, China; lsj930802@126.com (S.L.); xzhhuang@mail.neu.edu.cn (X.H.)

² Key Laboratory of Vibration and Control of Aero Propulsion Systems Ministry of Education of China, Northeastern University, Shenyang 110819, China

³ College of New Materials and New Energies, Shenzhen Technology University, Shenzhen 518118, China; yuzl@mail.neu.edu.cn

* Correspondence: lvhy@me.neu.edu.cn

Abstract: The propagation properties of waves in finite Timoshenko locally resonant (LR) beams resting on forced vibrations and periodically attached two-degree-of-freedom force-type resonators are studied by the wave-based analysis approach. By calculating the motion equations of the beam, the transmission and reflection matrices of waves at the resonator attached point are first derived, and the forced vibration response of the finite periodic beam is deduced by the wave-based approach. Several examples are also analyzed by the finite element method to verify the high accuracy of the developed wave-based analysis approach. Numerical results show that wider low-frequency band-gaps exist in this type of LR beams. It was also found that the resonator masses and spring stiffnesses caused different effects on the band-gap properties of the combined LR beam. The desired band-gap widths of the LR beam can be tuned by adjusting the mass blocks and spring stiffness in the resonators based on the results.

Keywords: Timoshenko LR beams; wave-based analysis approach; two-degree-of-freedom force-type resonators; low-frequency band-gaps



Citation: Lv, H.; Li, S.; Huang, X.; Yu, Z. Band-Gap Properties of Finite Locally Resonant Beam Suspended Periodically with Two-Degree-of-Freedom Force Type Resonators. *Crystals* **2021**, *11*, 716. <https://doi.org/10.3390/cryst11060716>

Academic Editors: Giuseppe Greco and M. Siva Pratap Reddy

Received: 13 May 2021
Accepted: 17 June 2021
Published: 21 June 2021

Publisher's Note: MDPI stays neutral with regard to jurisdictional claims in published maps and institutional affiliations.



Copyright: © 2021 by the authors. Licensee MDPI, Basel, Switzerland. This article is an open access article distributed under the terms and conditions of the Creative Commons Attribution (CC BY) license (<https://creativecommons.org/licenses/by/4.0/>).

1. Introduction

The propagation of acoustic and elastic waves in periodic structures, known as phononic crystals (PCs) and acoustics/elastic metamaterials (AMs/EMs) [1,2], has attracted growing interest in recent years. This structure can be designed and manufactured to cease the propagation of flexural waves in specific frequency bounds, known as band-gaps. This property allows for potential applications as acoustic or vibration devices [3–9]. Recently, the propagation of flexural waves along AMs/EMs has been studied by many researchers [10–13]. Among them, as a continuous–discrete structure, LR beams can effectively achieve vibration attenuation, where resonators are one or several spring-mass systems coupled with a continuous Euler or Timoshenko beam, with several potential applications in mechanical and structural engineering [14,15].

LR beams are often regarded as infinite systems. The existing analysis methods of the band-gap properties of LR beams mainly concern the transfer matrix method (TMM) [16,17], spectral element method [18], and finite element method (FEM) [19,20]. Yu et al. analyzed the low-frequency flexural wave band-gaps of Euler–Bernoulli and Timoshenko beams [11,12]; the dispersive relation of flexural waves was derived by using the TMM and the frequency response function (FRF) of a finite periodic system was calculated by the FEM. Liu and Hussein [21] improved the TMM to examine the trend of the frequency band structure of an LR beam modified by the spring constant or mass of local resonators, and the transition criterion was established by observing the transition between LR and Bragg

band-gaps. Liang [22] proposed an improved differential quadrature method to obtain the band-gap properties of a Euler–Bernoulli LR beam with spring-mass resonators. On the basis of these methods, various infinite periodic structures of LR beams have been constructed and studied for their band-gap properties theoretically and experimentally [23,24]. However, the boundary conditions are lacking in the analysis of infinite structures, and the engineering structures cannot be infinite. Thus, the analysis of the band-gap properties of finite structures plays an important part in real engineering applications. The FEM is the most widely applied method in vibration analysis of the finite LR beams [19,20,25]. Although the FEM can accurately evaluate the band-gap properties of various dimensions and shapes of LR beams, their time consumption and commercially expensive prices seriously limit wider use.

In recent years, many researchers have become more and more interested in a wave-based vibration analysis approach for finite LR beams. By using the availability of transmission, reflection, and transmission matrices, Mei and Mace [26] first derived the transmission and reflection matrices for different discontinuities on Timoshenko beams. Thus, the wave-based vibration analysis approach became more systematic and simple. Then, the wave-based vibration analysis approach was developed for the vibration analysis of LR beams carried out with periodic uncoupled force-moment resonators [27]. The wave-based vibration analysis approach can not only realize the complex vibration analysis of distributed structures, but is also efficient for combined distributed and discrete systems, offering benchmarks for numerical methods [28,29].

In this study, for finite Timoshenko LR beams combined with periodic coupled 2-DOF spring-mass systems, a wave-based vibration analysis approach is developed for forced vibration analysis. The transmission and reflection matrices at the 2-DOF force-type resonator attached point are first derived and assembled as a module with MATLAB software to be used for the calculations of forced response and band-gap properties of the LR beam. Here, the module can be called and modified easily by modeling the LR structure, which significantly simplifies the design work for LR structures. Several examples of analysis show that the proposed method is an efficient and accurate vibration analysis approach for finite periodical LR beams, and can be used as a paradigm. Finally, with the vibration analysis of the LR beam suspended with different resonators using the developed wave-based vibration analysis approach, we also analyzed how the mass block value and the spring stiffness of resonator influence the band-gap properties of the finite LR beam.

This paper is organized as follows: In Section 2, the equations of motion and wave propagation are presented. By considering the applied forces caused by the resonators when injecting waves into the host beam, the relationship between the propagation and reflection of the bending wave components at the 2-DOF force-type resonator attached point are obtained. In Section 3, the developed wave approach is applied for forced vibration analysis of an LR beam suspended periodically with eight 2-DOF force-type resonators. The calculation accuracy of the developed wave-based vibration analysis approach is verified by several numerical examples in Section 4 and the effects of mass and spring stiffness of the resonator on the band-gap properties of finite LR beams are studied in detail. Conclusions are drawn in Section 5.

Notation

The symbols used in this paper are listed in Table 1, and Table 2 summarizes the key abbreviations commonly used in this paper.

Table 1. Notations and definitions.

Notation	Definition
ρ	Mass density
E	Young's modulus
G	Shear modulus
A	Cross-sectional area
I	Area moment of inertia
κ	Shear coefficient
k	Spring stiffness
L	Lattice constant
w	Transverse deflection
u	Longitudinal deflection
ψ	Total bending
ω	Frequency
m	Resonator mass

Table 2. List of key acronyms used in this paper.

Acronym	Expansion
LR	Locally resonant
AMs	Acoustics metamaterials
EMs	Elastic metamaterials
TMM	Transfer matrix method
FEM	Finite element method
FRF	Frequency response function
LR	Locally resonant

2. Wave-Based Analysis Approach

2.1. Overview

In accordance with Ref. [30], the equations of motion governing bending, rotational, and longitudinal vibration for Timoshenko beams are:

$$GA\kappa\left(\frac{\partial\psi(x,t)}{\partial x} - \frac{\partial^2 w(x,t)}{\partial x^2}\right) + \rho A \frac{\partial^2 w(x,t)}{\partial t^2} = q(x,t) \quad (1)$$

$$EI \frac{\partial^2 \psi(x,t)}{\partial x^2} + GA\kappa\left(\frac{\partial w(x,t)}{\partial x} - \psi(x,t)\right) - \rho I \frac{\partial^2 \psi(x,t)}{\partial t^2} = 0 \quad (2)$$

$$\rho A \frac{\partial^2 u(x,t)}{\partial t^2} - EA \frac{\partial^2 u(x,t)}{\partial x^2} = p(x,t) \quad (3)$$

where x represents the position along the beam's neutral axis, t is time, $w(x,t)$ is the transverse deflection, and $u(x,t)$ is the longitudinal deflection. $\psi(x,t)$ denotes the total bending cross-sectional rotational angle, and $\frac{\partial w(x,t)}{\partial x}$ is the slope of the centerline of the beam. $\frac{\partial w(x,t)}{\partial x} - \psi(x,t)$ is the shear angle. $p(x,t)$ and $q(x,t)$ are the applied longitudinal and transverse forces on per unit length, respectively. Material properties are as follows: mass density ρ , Young's modulus E , and shear modulus G . Geometrical properties are: cross-sectional area A , area moment of inertia I , and shear coefficient κ , respectively.

The expressions of shear force $V(x,t)$, bending moment $M(x,t)$, and longitudinal force $F(x,t)$, respectively, are:

$$V(x,t) = GA\kappa\left(\frac{\partial w(x,t)}{\partial x} - \psi(x,t)\right) \quad (4)$$

$$M(x,t) = EI \frac{\partial \psi(x,t)}{\partial x} \quad (5)$$

$$F(x, t) = EA \frac{\partial u(x, t)}{\partial x} \tag{6}$$

We consider the absence of loading and the suppression of time dependence $e^{i\omega t}$; the solutions to the free wave propagation Equations (1)–(3) are expressed as:

$$w(x, t) = a_1^+ e^{-ik_1x} + a_2^+ e^{k_2x} + a_1^- e^{ik_1x} + a_2^- e^{k_2x} \tag{7}$$

$$\psi(x, t) = -iPa_1^+ e^{-ik_1x} - Na_2^+ e^{-k_2x} + iPa_1^- e^{ik_1x} + Na_2^- e^{k_2x} \tag{8}$$

$$u(x, t) = c^+ e^{-ik_3x} + c^- e^{ik_3x} \tag{9}$$

where a_1, a_2, c are the amplitude of the propagating flexural wave, the near-field flexural wave, and the propagating longitudinal wave, respectively. The superscripts + or – represent the forward- or backward-propagating waves. k_1, k_2, k_3 denote the three wavenumbers. iP and N relate the rotational solution to the transverse displacement solution as:

$$P = k_1 \left(1 - \frac{\omega^2}{k_1^2 C_s^2} \right), \quad N = k_2 \left(1 + \frac{\omega^2}{k_2^2 C_s^2} \right) \tag{10}$$

The relations of wavenumber–frequency dispersion are obtained as:

$$k_1 = \sqrt{\frac{1}{2} \left[\left(\frac{1}{C_s} \right)^2 + \left(\frac{C_r}{C_b} \right)^2 \right] \omega^2 + \sqrt{\left(\frac{\omega}{C_b} \right)^2 + \frac{1}{4} \left[\left(\frac{1}{C_s} \right)^2 - \left(\frac{C_r}{C_b} \right)^2 \right]^2 \omega^4}} \tag{11}$$

$$k_2 = \sqrt{-\frac{1}{2} \left[\left(\frac{1}{C_s} \right)^2 + \left(\frac{C_r}{C_b} \right)^2 \right] \omega^2 + \sqrt{\left(\frac{\omega}{C_b} \right)^2 + \frac{1}{4} \left[\left(\frac{1}{C_s} \right)^2 - \left(\frac{C_r}{C_b} \right)^2 \right]^2 \omega^4}} \tag{12}$$

$$k_3 = \sqrt{\frac{E}{\rho} \omega^2} \tag{13}$$

where the wave speeds for bending, shear and rotation are expressed as:

$$C_s = \sqrt{\frac{GA\kappa}{\rho A}}, \quad C_b = \sqrt{\frac{EI}{\rho A}}, \quad C_r = \sqrt{\frac{\rho I}{\rho A}} \tag{14}$$

Note that, for the LR beam suspended with periodic 2-DOF force-type resonators investigated in this paper, only bending vibrations were involved.

2.2. Propagation Matrix

Between discontinuities, Equations (7)–(9) represents the exact state of wave propagation at a single frequency in a uniform beam. Here, we consider two points—A and B—of a beam falling between discontinuities and separated by a distance x , as shown in Figure 1. Since only bending vibrations are involved in the LR beam, the propagation matrix can be defined as:

$$\mathbf{b}^+ = \mathbf{f}(x) \mathbf{a}^+, \quad \mathbf{a}^- = \mathbf{f}(x) \mathbf{b}^- \tag{15}$$

where

$$\mathbf{a}^+ = \begin{bmatrix} a_1^+ \\ a_2^+ \end{bmatrix}, \quad \mathbf{a}^- = \begin{bmatrix} a_1^- \\ a_2^- \end{bmatrix}, \quad \mathbf{b}^+ = \begin{bmatrix} b_1^+ \\ b_2^+ \end{bmatrix}, \quad \mathbf{b}^- = \begin{bmatrix} b_1^- \\ b_2^- \end{bmatrix} \tag{16}$$

\mathbf{a}^+ and \mathbf{a}^- are the wave coefficients for forward- and backward-propagating waves at point A. \mathbf{b}^+ and \mathbf{b}^- are wave coefficients at point B.

$$\mathbf{f}(x) = \begin{bmatrix} e^{-ik_1x} & 0 \\ 0 & e^{-k_2x} \end{bmatrix} \tag{17}$$

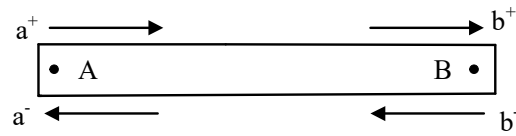


Figure 1. Wave propagation at two points separated by a distance x along a uniform beam.

2.3. Reflection at a Free Boundary

The boundary condition for the LR beam investigated in this paper is free-free ends. Thus, the transverse force and bending moment must all vanish. The relationship between the incident waves a^+ and the reflected waves a^- is expressed with a reflection matrix as:

$$a^- = r_f a^+ \tag{18}$$

where

$$r_f = \begin{bmatrix} \frac{-Pk_1(-N+k_2)+ik_2N(k_1-P)}{Pk_1(-N+k_2)+ik_2N(k_1-P)} & \frac{2Nk_2(-N+k_2)}{Pk_1(-N+k_2)+ik_2N(k_1-P)} \\ \frac{2iPk_1(-P+k_1)}{Pk_1(-N+k_2)+ik_2N(k_1-P)} & \frac{Pk_1(-N+k_2)-ik_2N(k_1-P)}{Pk_1(-N+k_2)+ik_2N(k_1-P)} \end{bmatrix} \tag{19}$$

2.4. Applied Forces and Moments

Figure 2 depicts the waves a and b generated by the external force applied at $x = 0$. Continuity and equilibrium conditions can be obtained as:

$$b^+ - a^+ = f \tag{20}$$

$$b^- - a^- = -f \tag{21}$$

where the vectors of the excited wave amplitudes are:

$$f = \begin{bmatrix} iN \\ P \end{bmatrix} \frac{F}{GA\kappa(k_2P - k_1N)} \tag{22}$$

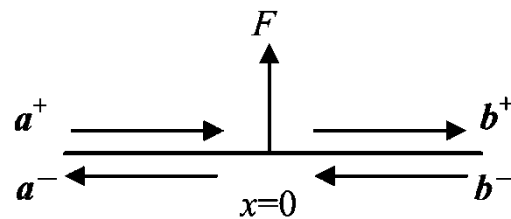


Figure 2. Waves generated by external force.

2.5. Transmission and Reflection at the 2-DOF Force-Type Resonator Attached Point

The LR beam suspended with 2-DOF force-type resonators is depicted in Figure 3, where m_1 and m_2 are the masses of the resonators, k_A and k_B are the stiffnesses of two linear elastic springs, and L is the lattice constant of the periodic structure (distance between two adjacent 2-DOF force-type resonators).

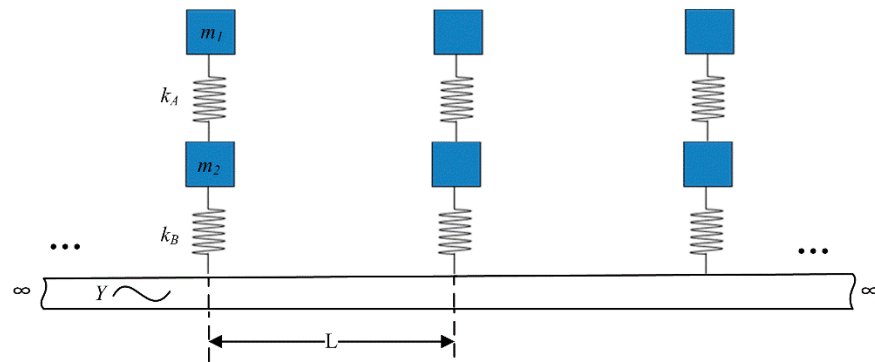


Figure 3. A beam with periodic 2-DOF force-type resonators.

Figure 4 presents the free body diagram of a single resonator on the beam. In the figure, w_{mA} and w_{mB} denote the transverse deflections of the mass blocks m_1 and m_2 , respectively. F_A is the force caused by the spring between the mass blocks m_1 and m_2 . Similarly, F_B is the force caused by the spring between the mass block m_2 and the host beam. w , u , and ψ are the transverse deflection, axial deflection and angular rotation of the host beam at the point resonator attached. F is the force of the resonator applied on the host beam. Here, for the 2-DOF force-type resonator, $F = F_B$. Note that, the transverse deflection w is only involved here because the 2-DOF force-type resonator applies transverse force only to the host beam.

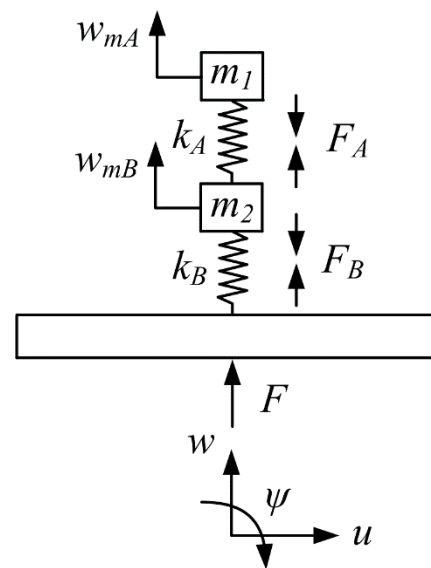


Figure 4. Free body diagram of a cell of resonators.

As shown in Figure 4, the equation of motion of the resonator can be written as:

$$-F_A = m_1 \ddot{w}_{mA} \tag{23}$$

$$F_A - F_B = m_2 \ddot{w}_{mB} \tag{24}$$

where

$$F_A = k_A (w_{mA} - w_{mB}) \tag{25}$$

$$F_B = k_B (w_{mB} - w) \tag{26}$$

Combining Equations (23)–(26), and considering the motion of the system is time harmonic with frequency ω , the displacements of the mass blocks w_{mA} and w_{mB} can be expressed in terms of the deflection at the attachment point w as:

$$w_{mA} = \frac{-k_A k_B}{k_A m_1 \omega^2 + k_B m_1 \omega^2 + k_A m_2 \omega^2 - k_A k_B} w \tag{27}$$

$$w_{mB} = \frac{k_B m_1 \omega^2 - k_A k_B}{k_A m_1 \omega^2 + k_B m_1 \omega^2 + k_A m_2 \omega^2 - k_A k_B} w \tag{28}$$

Then, the forces F_A and F_B between the mass blocks and host beam can be obtained from Equations (25)–(28):

$$F_A = r_1 w \tag{29}$$

$$F = F_B = r_2 w \tag{30}$$

where

$$r_1 = \frac{-k_A k_B m_1 \omega^2}{k_A m_1 \omega^2 + k_B m_1 \omega^2 + k_A m_2 \omega^2 - k_A k_B}$$

$$r_2 = \frac{-k_A k_B (m_1 + m_2) \omega^2}{k_A m_1 \omega^2 + k_B m_1 \omega^2 + k_A m_2 \omega^2 - k_A k_B}$$

As in Ref. [31], the applied forces caused by the resonators can be considered as injecting waves into the host beam. Substituting the expression of transverse force F in Equation (30) into Equation (22), and combining Equations (7)–(9), (20), (21), one can obtain the relations of vibration waves at the point resonator attached,

$$\begin{bmatrix} A_{11} & A_{12} \\ A_{21} & A_{22} \end{bmatrix} \begin{bmatrix} a^+ \\ a^- \end{bmatrix} + \begin{bmatrix} B_{11} & B_{12} \\ B_{21} & B_{22} \end{bmatrix} \begin{bmatrix} b^+ \\ b^- \end{bmatrix} = 0 \tag{31}$$

where the coefficient matrices in Equation (31) are

$$A_{11} = \begin{bmatrix} iN\beta r_2 + 1 & iN\beta r_2 \\ P\beta r_2 & P\beta r_2 + 1 \end{bmatrix}$$

$$A_{12} = \begin{bmatrix} iN\beta r_2 & iN\beta r_2 \\ P\beta r_2 & P\beta r_2 \end{bmatrix}$$

$$A_{21} = \begin{bmatrix} -iN\beta r_2 & -iN\beta r_2 \\ -P\beta r_2 & -P\beta r_2 \end{bmatrix}$$

$$A_{22} = \begin{bmatrix} -iN\beta r_2 + 1 & -iN\beta r_2 \\ -P\beta r_2 & -P\beta r_2 + 1 \end{bmatrix}$$

$$B_{11} = B_{22} = \begin{bmatrix} -1 & 0 \\ 0 & -1 \end{bmatrix}$$

$$B_{12} = B_{21} = \begin{bmatrix} 0 & 0 \\ 0 & 0 \end{bmatrix}$$

$$\beta = \frac{1}{2(GA\kappa)(k_2 P - k_1 N)}$$

3. Vibration Analysis with Wave-Based Approach

Figure 5 denotes a LR beam suspended periodically with eight 2-DOF force-type resonators with the involved wave components. As shown in the figure, the resonators are attached at points B, C, D, E, F, H, J, and K. The lattice constant of the structure is L . Two ends of the host beam are freely supported. The external force is applied at point G with the generated waves g_{11}^+ , g_{11}^- , g_{12}^+ and g_{12}^- . The distance between point G and the

left end of the host beam (point A) is L_{11} , and the distance from point G to point B (the first resonator attached point) is L_{12} . The length from the last resonator to the right end of the host beam (point M) is L . According to the propagation, transmission, and reflection relations described in Section 2, the relations of waves at discontinuities of the LR beam can be obtained as follows.

At eight resonator attachment points B, C, D, E, F, H, J, and K:

$$\begin{bmatrix} A_{11} & A_{12} \\ A_{21} & A_{22} \end{bmatrix} \begin{bmatrix} b_1^+ \\ b_1^- \end{bmatrix} + \begin{bmatrix} B_{11} & B_{12} \\ B_{21} & B_{22} \end{bmatrix} \begin{bmatrix} b_2^+ \\ b_2^- \end{bmatrix} = 0 \quad (32)$$

$$\begin{bmatrix} A_{11} & A_{12} \\ A_{21} & A_{22} \end{bmatrix} \begin{bmatrix} c_1^+ \\ c_1^- \end{bmatrix} + \begin{bmatrix} B_{11} & B_{12} \\ B_{21} & B_{22} \end{bmatrix} \begin{bmatrix} c_2^+ \\ c_2^- \end{bmatrix} = 0 \quad (33)$$

$$\begin{bmatrix} A_{11} & A_{12} \\ A_{21} & A_{22} \end{bmatrix} \begin{bmatrix} d_1^+ \\ d_1^- \end{bmatrix} + \begin{bmatrix} B_{11} & B_{12} \\ B_{21} & B_{22} \end{bmatrix} \begin{bmatrix} d_2^+ \\ d_2^- \end{bmatrix} = 0 \quad (34)$$

$$\begin{bmatrix} A_{11} & A_{12} \\ A_{21} & A_{22} \end{bmatrix} \begin{bmatrix} e_1^+ \\ e_1^- \end{bmatrix} + \begin{bmatrix} B_{11} & B_{12} \\ B_{21} & B_{22} \end{bmatrix} \begin{bmatrix} e_2^+ \\ e_2^- \end{bmatrix} = 0 \quad (35)$$

$$\begin{bmatrix} A_{11} & A_{12} \\ A_{21} & A_{22} \end{bmatrix} \begin{bmatrix} f_1^+ \\ f_1^- \end{bmatrix} + \begin{bmatrix} B_{11} & B_{12} \\ B_{21} & B_{22} \end{bmatrix} \begin{bmatrix} f_2^+ \\ f_2^- \end{bmatrix} = 0 \quad (36)$$

$$\begin{bmatrix} A_{11} & A_{12} \\ A_{21} & A_{22} \end{bmatrix} \begin{bmatrix} h_1^+ \\ h_1^- \end{bmatrix} + \begin{bmatrix} B_{11} & B_{12} \\ B_{21} & B_{22} \end{bmatrix} \begin{bmatrix} h_2^+ \\ h_2^- \end{bmatrix} = 0 \quad (37)$$

$$\begin{bmatrix} A_{11} & A_{12} \\ A_{21} & A_{22} \end{bmatrix} \begin{bmatrix} j_1^+ \\ j_1^- \end{bmatrix} + \begin{bmatrix} B_{11} & B_{12} \\ B_{21} & B_{22} \end{bmatrix} \begin{bmatrix} j_2^+ \\ j_2^- \end{bmatrix} = 0 \quad (38)$$

$$\begin{bmatrix} A_{11} & A_{12} \\ A_{21} & A_{22} \end{bmatrix} \begin{bmatrix} k_1^+ \\ k_1^- \end{bmatrix} + \begin{bmatrix} B_{11} & B_{12} \\ B_{21} & B_{22} \end{bmatrix} \begin{bmatrix} k_2^+ \\ k_2^- \end{bmatrix} = 0 \quad (39)$$

At free support boundaries A and M:

$$a^+ = r_f a^- \quad (40)$$

$$m^- = r_f m^+ \quad (41)$$

Ten pairs of propagation relations along the beam elements are included for the LR structure: AG, GB, BC, CD, DE, EF, FH, HJ, JK, and KM.

Along AG

$$g_{11}^+ = f(L_{11})a^+, \quad a^- = f(L_{11})g_{11}^- \quad (42)$$

Along GB

$$b_1^+ = f(L_{12})g_{12}^+, \quad g_{12}^- = f(L_{12})b_1^- \quad (43)$$

Along BC

$$c_1^+ = f(L)b_2^+, \quad b_2^- = f(L)c_1^- \quad (44)$$

Along CD

$$d_1^+ = f(L)c_2^+, \quad c_2^- = f(L)d_1^- \quad (45)$$

Along DE

$$e_1^+ = f(L)d_2^+, \quad d_2^- = f(L)e_1^- \quad (46)$$

Along EF

$$f_1^+ = f(L)e_2^+, \quad e_2^- = f(L)f_1^- \quad (47)$$

Along FH

$$h_1^+ = f(L)f_2^+, \quad f_2^- = f(L)h_1^- \quad (48)$$

Along HJ

$$j_1^+ = f(L)h_2^+, \quad h_2^- = f(L)j_1^- \quad (49)$$

Along JK

$$k_1^+ = f(L)j_2^+, j_2^- = f(L)k_1^- \tag{50}$$

Along KM

$$m^+ = f(L)k_2^+, k_2^- = f(L)m^- \tag{51}$$

The relations between the external force and the generated wave amplitudes are:

$$g_{12}^+ - g_{11}^+ = q \tag{52}$$

$$g_{12}^- - g_{11}^- = -q \tag{53}$$

Combining Equations (32)–(51) and writing into matrix algebraic form gives:

$$A_f z_f = F \tag{54}$$

where A_f is an 80×80 coefficient matrix, z_f is an 80×1 component vector, and F is an 80×1 vector holding the external transverse forces to the host beam.

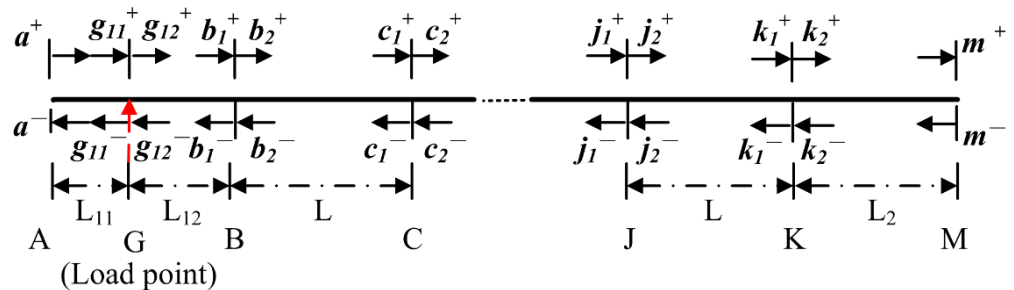


Figure 5. Wave analysis of a finite LR beam.

4. Numerical Results and Discussion

Consider the aluminum LR beam suspended with eight periodic 2-DOF force-type resonators such as the structure in Figure 3. The parameters are: the Young’s modulus $E = 70\text{G N/m}^2$, the Poisson’s ratio $\nu = 0.33$, and the shear modulus [2], which is calculated by $G = E/2(1 + \nu)$. The mass density $\rho = 2700\text{ kg/m}^3$. The cross-section of the beam elements is $3 \times 10^{-3} \times 1 \times 10^{-2}\text{ m}^2$. The shear coefficient can be obtained from $\kappa = 10(1 + \nu)/(12 + 11\nu)$. The lattice constant is L . The loading is applied at the position $L_{11} = 0.01\text{ m}$ from the left end of the host beam, and the $L_{12} = 0.09\text{ m}$. The distance between the measured point and the right end of the host beam is $L_m = 0.01\text{ m}$, and the last resonator has a distance of $L_2 = 0.1\text{ m}$ away from the right end of the host beam.

First of all, the effect of the number of resonators on the band-gap of the LR beam is investigated with the newly developed wave-based analysis approach described above. Figure 6 shows the transmission curves of LR beams with different numbers of resonators N , in which the resonator parameters are the same: $k_A = k_B = 1.6384 \times 10^4\text{ N/m}$, $m_1 = m_2 = 20.054\text{ g}$, $L = 0.1\text{ m}$. It is obvious that the transmittance drops inside the two band-gaps increase with an increasing number of resonators. Moreover, the bandwidths of the two band-gaps increase with an increasing number of resonators as well until $N = 8$. When the number of resonators increases to 10, the drop in transmittance increases, while the bandwidths of the band-gaps remain the same. Since the bandwidth of the band-gap is the most important characteristic of the LR beam, the optimal number of resonators is $N = 8$, obtained from Figure 6. In this paper, the number of resonators was chosen as eight for further investigations.

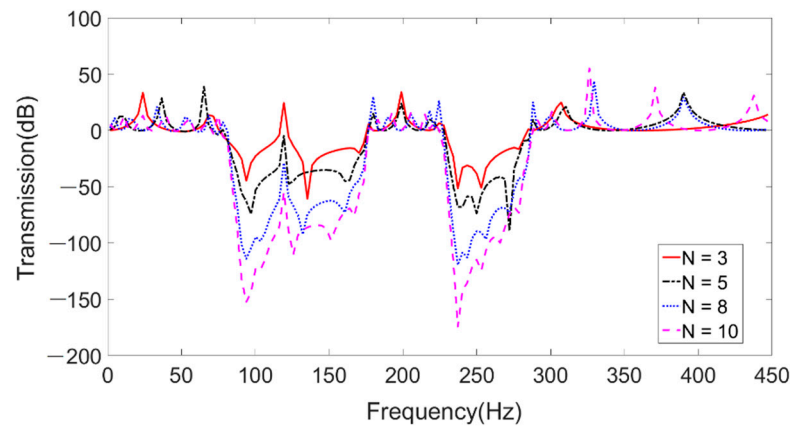


Figure 6. The FRF of the LR beam with different number of resonators $N = 3, 5, 8, 10$.

Figure 7 shows the influence of the lattice constant L (location of resonators) on the band-gaps of the LR beam. Similarly, the resonator parameters are: $k_A = k_B = 1.6384 \times 10^4$ N/m, $m_1 = m_2 = 20.054$ g. As shown in Figure 7, the bandwidth of the lower frequency band-gap remains the same as the lattice constant L is increased; meanwhile, the band-gap moves to a lower frequency range. In addition, the bandwidth and frequency range of the higher frequency band-gap both decrease with the increase in lattice constant L .

The effect of the total mass of the eight resonators on the band structure of the LR beam is acquired in Figure 8. The resonator parameters are: $L = 0.1$ m, $k_A = k_B = 1.6384 \times 10^4$ N/m, and $m_1 = m_2$. As expected, the bandwidths of the higher frequency band-gap increase as the total mass of the resonators increases; meanwhile, the band-gap moves to a lower frequency range. However, the width of the lower frequency band-gap is maintained with the increase in total mass, while the band-gap moves to a lower frequency.

To further investigate the influences of mass blocks m_1, m_2 and spring stiffnesses k_A, k_B of the resonator on the band-gap width of the LR beam suspended with eight periodic 2-DOF force-type resonators, the band-gap widths of the LR beam with different resonator structures are calculated. The mass blocks m_1, m_2 and spring stiffnesses k_A, k_B of all selected resonators are listed in Table 3. The lattice constant $L = 0.1$ m.

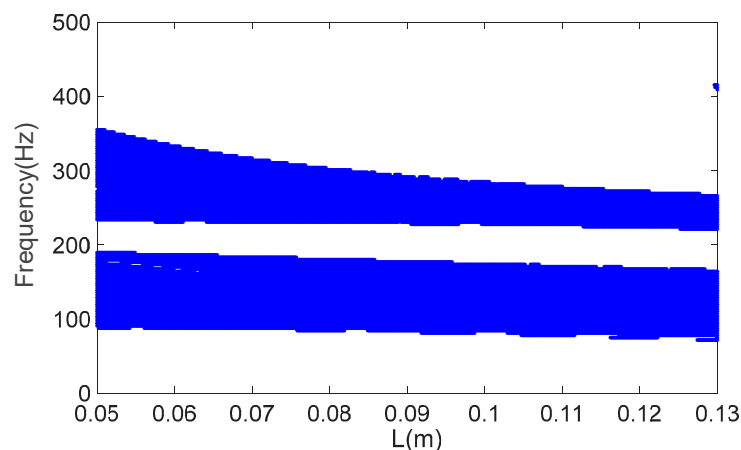


Figure 7. The band-gap widths vary with lattice constant L .

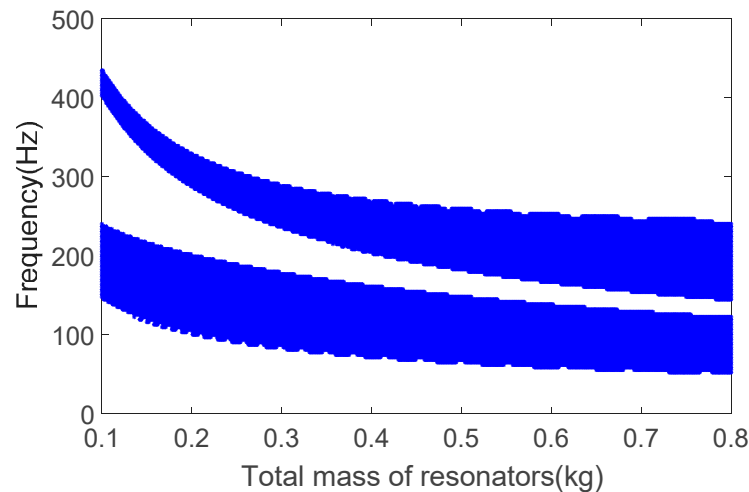


Figure 8. The band-gap widths vary with total mass of resonators.

Table 3. Schemes of mass distribution and spring stiffness of resonators.

	Case	m_1 (g)	m_2 (g)	k_A (N/m)	k_B (N/m)	Relations
Scheme 1	Case 1	2~20	20~200	8.1921×10^3	8.1921×10^3	$m_1/m_2 = 0.1$
	Case 2	20~200	2~20	8.1921×10^3	8.1921×10^3	$m_1/m_2 = 10$
Scheme 2	Case 3	10	10	2000~12,000	8000~48,000	$k_A/k_B = 0.25$
	Case 4	10	10	8000~48,000	2000~12,000	$k_A/k_B = 4$

With the newly developed wave-based analysis approach, the band-gap widths of all cases are obtained and the calculation results are shown in Figures 9 and 10. It can be seen directly from Figure 9 that the band-gap width increases with the mass of the resonator; meanwhile, the band-gap moves to a lower frequency. The mass blocks m_1 and m_2 of resonator have the opposite mass ratio in case 1 and case 2. By comparing the band-gap properties in Figure 9a,b, it can be seen that a larger mass proportion of m_2 can realize better band-gap properties with the sum mass of resonator masses m_1 and m_2 unchanged. The variation trend of band-gap width with spring stiffness is depicted in Figure 10. The two subfigures in Figure 10 show the band-gap width increases with the spring stiffness, and the band-gap moves to a higher frequency in the meantime. The opposite spring stiffness ratios are selected in case 3 and case 4. Through a comparative analysis of Figure 10a,b, the band-gap width with spring stiffness ratio $k_A/k_B = 0.25$ is much wider than the opposite spring stiffness ratio $k_A/k_B = 4$, which shows that the larger spring stiffness k_B should be selected for a wider band-gap width. All these results show that the mass and spring stiffness of the resonator are positively correlated with the band-gap width. It should also be noted that when larger values for resonator mass m_2 and spring stiffness k_B are selected compared to mass m_1 and stiffness k_A , it is easier to widen the band-gap width in a low-frequency range.

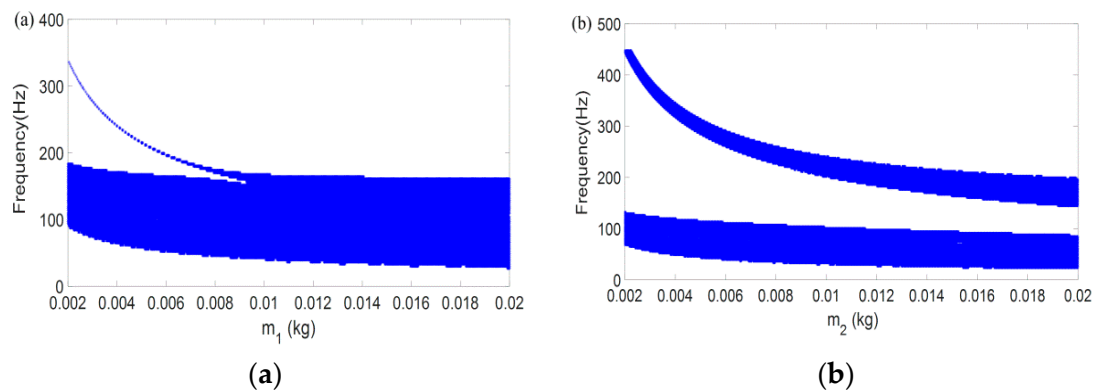


Figure 9. The band-gap widths vary with mass distribution with the same spring stiffness. (a) The band-gap widths vary with m_1 of Case 1; (b) The band-gap widths vary with m_2 of Case 2.

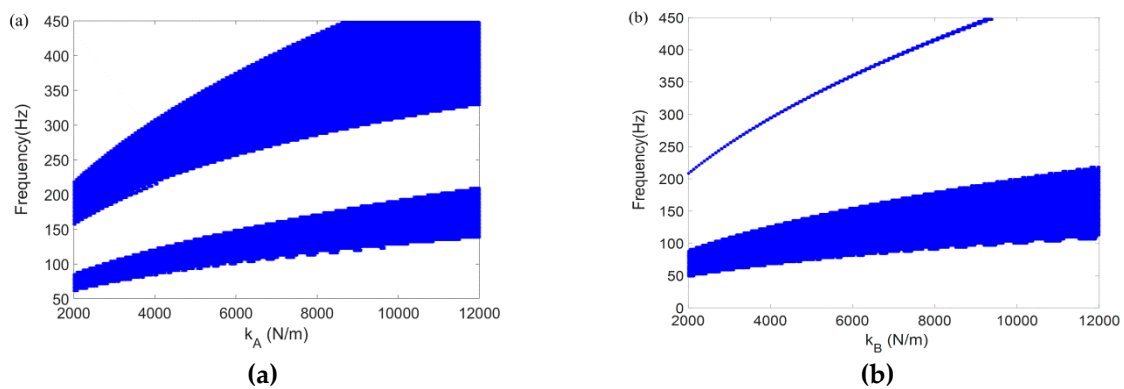


Figure 10. The band-gap widths vary with spring stiffness with the same mass distribution. (a) The band-gap widths vary with k_A of Case 3; (b) The band-gap widths vary with k_B of Case 4.

In order to verify the calculation accuracy of the wave-based analysis approach for this kind of finite periodic LR beam, several sets of resonators were selected. The physical parameters, including the first two natural frequencies of the resonators, are listed in Table 4. The band-gap widths are calculated by the wave-based analysis approach and FEM (ANSYS Workbench), respectively.

Table 4. Different mass and spring stiffness of resonator samples.

Resonator	m_1 (g)	m_2 (g)	k_A (N/m)	k_B (N/m)	Mode 1 (Hz)	Mode 2 (Hz)
Resonator 1	10.027	10.027	8.1921×10^3	8.1921×10^3	88.97	232.8
Resonator 2	20.054	10.027	1.6384×10^4	8.1921×10^3	74.48	277.9
Resonator 3	10.027	20.054	8.1921×10^3	1.6384×10^4	101.7	203.5
Resonator 4	20.054	20.054	1.6384×10^4	1.6384×10^4	88.91	232.77

As shown in Table 4, the resonator samples we selected have some relations—the values of mass block m_1 and spring stiffness k_A in resonator 2 are two times greater than resonator 1, and resonator 3 has two times the mass m_2 and stiffness k_B than resonator 1. For resonator 4, m_1 , m_2 , k_A , and k_B are all two times greater than resonator 1. As already known from Figures 9 and 10, the band-gap width is greater with the increase in resonator mass and spring stiffness. Here, we increase k_A and k_B along with m_1 and m_2 , respectively, to make sure the natural frequencies of the resonators are close to each other. The effect of (a) m_1 and k_A , and (b) m_2 and k_B on the band-gaps of the LR beam is discussed in the results later.

In the simulation, two ends of the host beam were free supported. Figure 11 depicts one of the geometrical models for FEM simulation. The red arrow in the figure represents

the harmonic force excitation with frequency range from 0 to 450 Hz applied on the loading site of the host beam in the y direction. The loading site was the point with a distance $L_{11} = 0.01$ m from the left end of the host beam. Meanwhile, the measured point was the point with a distance $L_m = 0.01$ m from the right end.

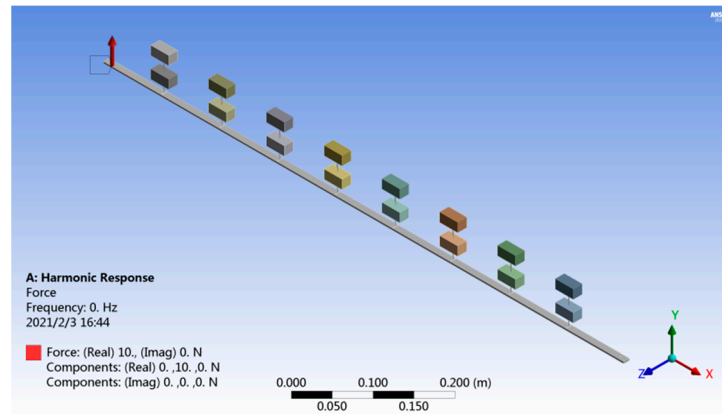


Figure 11. Structural model in the FEM simulation.

The frequency response function (FRF) of the finite LR beam suspended with different sets of resonators, respectively, is analyzed through the newly developed wave-based vibration analysis approach and FEM, as is shown in Figure 12. It can be seen from the comparisons that the FRF curves of the periodic beam calculated by the wave-based vibration analysis approach and FEM are very close to each other. The fitness of the FRF results calculated by the two methods verifies the correctness of the wave-based analysis method proposed to calculate the band-gap properties of the finite periodic LR beam.

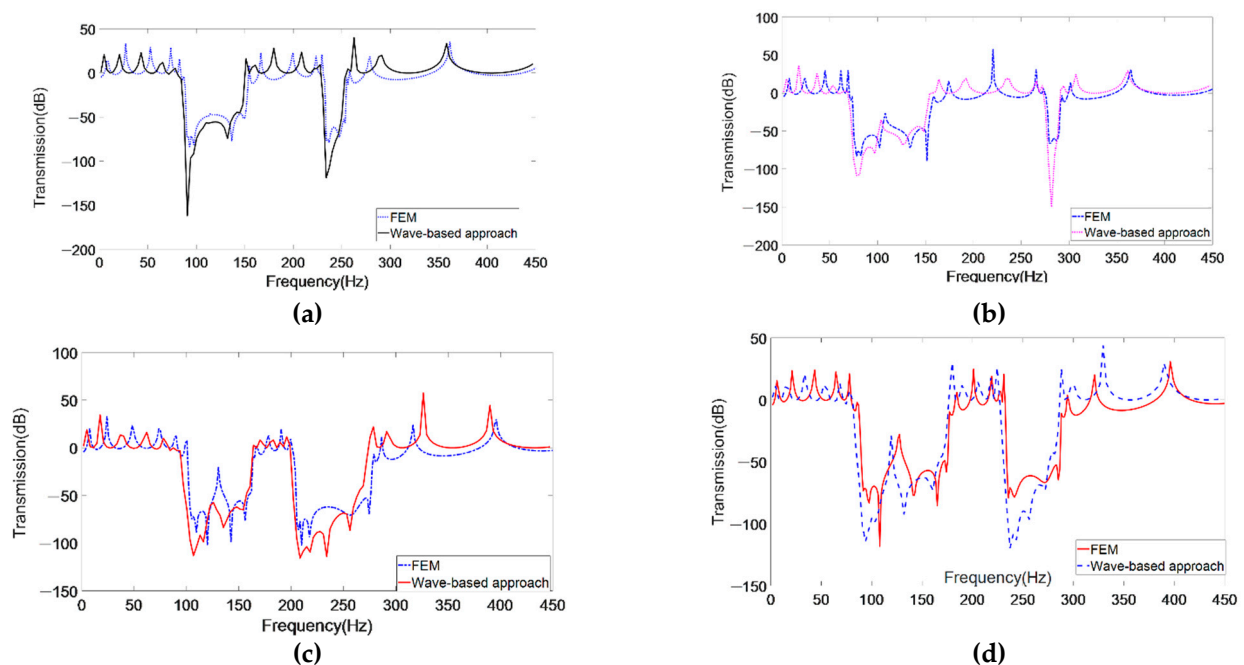


Figure 12. The FRF of the LR beam using wave-based vibration analysis approach and FEM. (a) The comparison of FRF with resonator 1; (b) The comparison of FRF with resonator 2; (c) The comparison of FRF with resonator 3; (d) The comparison of FRF with resonator 4.

For further insight into the propagation characteristics of the finite periodic LR beam with different resonators, and how the mass and spring stiffness of the resonator influence the band-gap width, the FRF curves of the LR beams with these four different sets of

resonators are plotted in Figure 13. From Figure 13, we can find that the band-gap widths of all cases are wider than the one associated with resonator 1, and the degree of width is related to the mass distribution and spring stiffness of the resonators.

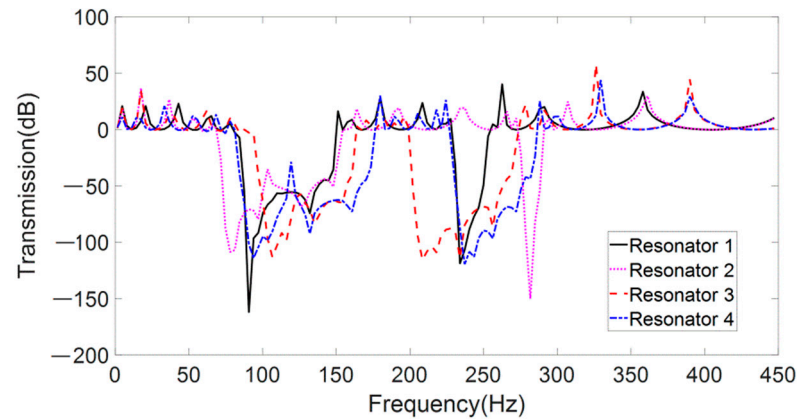


Figure 13. The FRFs of the LR beam suspended with different resonators.

In order to observe the effects of the mass distribution and spring stiffness of the resonator on the band-gap width more accurately, the band-gap widths and boundaries of the LR beam with different resonators are summarized in Table 5. The data in Table 5 show that the lower boundaries of the band-gaps are all around the first two natural frequencies of the resonators, respectively. As expected, the band-gap width broadens with the increase in resonator mass and spring stiffness. Furthermore, the increase in (a) m_1 and k_A , and (b) m_2 and k_B has different effects on the band-gaps. The band-gap width associated with resonator 2 in the lower frequency range is increased by 26.8% more than the one associated with resonator 1, which depicts that the increase in mass block m_1 and k_A is beneficial to widen the band-gap width in a lower frequency range. The band-gap width associated with resonator 3 in a higher frequency range is 3.14 times greater than the one associated with resonator 1. This result shows that it is effective to increase the mass block m_2 and k_B to widen the band-gap width in a higher frequency range. The mass blocks m_1 , m_2 and spring stiffnesses k_A , k_B in resonator 4 are two times greater than in resonator 1. The band-gap widths associated with resonator 4 increased by 40% in the lower frequency range and 157.07% in the higher frequency range compared to resonator 1. All these results illustrate a trend of variation in band-gap width associated with mass distribution and spring stiffness.

Table 5. Summary of band-gap widths.

Resonator	Lower Frequency Band-Gap (Hz)		Higher Frequency Band-Gap (Hz)	
	Region (Hz)	Width	Region (Hz)	Width
Resonator 1	[84.35, 148.01]	63.66	[230.77, 253.06]	22.29
Resonator 2	[71.62, 151.20]	79.58	[275.34, 288.07]	12.73
Resonator 3	[97.08, 160.75]	63.67	[202.13, 272.16]	70.03
Resonator 4	[84.35, 173.48]	89.13	[227.59, 284.89]	57.30

5. Conclusions

In this paper, the wave-based vibration analysis approach was employed and developed by solving forced vibrations of a finite LR beam suspended periodically with 2-DOF force-type resonators. Considering the applied force caused by the resonator when injecting the wave into the host beam, the reflection and transmission matrices at the 2-DOF force-type resonator attached point were derived, and the propagation characteristics of the Timoshenko beam periodically suspended with eight 2-DOF force-type resonators were

analyzed. The vibration analysis procedure is only a simple assembly of the involved reflection and transmission matrices, which shows the high efficiency of the derived analytical method in vibration analysis of finite LR beams. The band-gap properties of several examples were calculated with the developed wave-based analysis approach and FEM; good agreements with FEM results showed the high accuracy of the analytical method. Thus, the developed wave-based analysis approach can be used as a valuable tool in vibration analysis of finite LR beams. In particular, the influence of mass and spring stiffness of the resonators on band-gaps width of Timoshenko beams was investigated with different cases. It was found that the mass and spring stiffness m_1 and k_A of the resonator were in charge of the lower-frequency band-gap of the LR beam, while m_2 and k_B had more influence on the higher-frequency band-gap. The results in this paper provide guidance in the design of an LR beam for vibration attenuation in engineering practice.

Author Contributions: Conceptualization and methodology, H.L.; writing—original draft preparation, S.L.; supervision, X.H.; validation, Z.Y. All authors have read and agreed to the published version of the manuscript.

Funding: This work is supported by the National Natural Science Foundation of China (Grant No. 51975110), Liaoning Revitalization Talents Program (Grant No. XLYC1907171) and Fundamental Research Funds for the Central Universities (Grant No. N2003005 and N2003027).

Data Availability Statement: Not applicable.

Conflicts of Interest: The authors declare that they have no known competing financial interests or personal relationships that could have appeared to influence the work reported in this paper.

References

- Lu, M.-H.; Feng, L.; Chen, Y.-F. Phononic crystals and acoustic metamaterials. *Mater. Today* **2009**, *12*, 34–42. [\[CrossRef\]](#)
- Hussein, M.I.; Leamy, M.J.; Ruzzene, M. Dynamics of Phononic Materials and Structures: Historical Origins, Recent Progress, and Future Outlook. *Appl. Mech. Rev.* **2014**, *66*, 040802. [\[CrossRef\]](#)
- Kaina, N.; LeMoult, F.; Fink, M.; Lerosey, G. Negative refractive index and acoustic superlens from multiple scattering in single negative metamaterials. *Nat. Cell Biol.* **2015**, *525*, 77–81. [\[CrossRef\]](#)
- Farajpour, M.R.; Shahidi, A.R.; Farajpour, A. Resonant frequency tuning of nanobeams by piezoelectric nanowires under thermo-electro-magnetic field: A theoretical study. *Micro Nano Lett.* **2018**, *13*, 1627–1632. [\[CrossRef\]](#)
- Rohani, R.E.; Farajpour, M.R. Influence of taxol and CNTs on the stability analysis of protein microtubules. *J. Comput. Appl. Mech.* **2019**, *50*, 140–147. [\[CrossRef\]](#)
- Timorian, S.; Petrone, G.; De Rosa, S.; Franco, F.; Ouisse, M.; Bouhaddi, N. Spectral analysis and structural response of periodic and quasi-periodic beams. *Proc. Inst. Mech. Eng. Part C J. Mech. Eng. Sci.* **2019**, *233*, 7498–7512. [\[CrossRef\]](#)
- Errico, F.; Petrone, G.; Rosa, S.D.; Franco, F.; Ichchou, M. On the concept of embedded resonators for passive vibration control of tyres. *Proc. Inst. Mech. Eng. Part C J. Mech. Eng. Sci.* **2021**, 1–7. [\[CrossRef\]](#)
- Safarabadi, M.; Mohammadi, M.; Farajpour, A.; Goodarzi, M. Effect of surface energy on the vibration analysis of rotating nanobeam. *J. Solid Mech.* **2015**, *7*, 299–311.
- Lv, H.; Tian, X.; Wang, M.Y.; Li, D. Vibration energy harvesting using a phononic crystal with point defect states. *Appl. Phys. Lett.* **2013**, *102*, 034103. [\[CrossRef\]](#)
- An, X.; Lai, C.; Fan, H.; Zhang, C. 3D acoustic metamaterial-based mechanical metalattice structures for low-frequency and broadband vibration attenuation. *Int. J. Solids Struct.* **2020**, *191*, 293–306. [\[CrossRef\]](#)
- Yu, D.; Liu, Y.; Zhao, H.; Wang, G.; Qiu, J. Flexural vibration band gaps in Euler-Bernoulli beams with locally resonant structures with two degrees of freedom. *Phys. Rev. B* **2006**, *73*, 64301. [\[CrossRef\]](#)
- Yu, D.; Liu, Y.; Wang, G.; Zhao, H.; Qiu, J. Flexural vibration band gaps in Timoshenko beams with locally resonant structures. *J. Appl. Phys.* **2006**, *100*, 124901. [\[CrossRef\]](#)
- Ghayesh, M.H.; Farajpour, A. Vibrations of shear deformable FG viscoelastic microbeams. *Microsyst. Technol.* **2018**, *25*, 1387–1400. [\[CrossRef\]](#)
- Zhu, R.; Liu, X.; Hu, G.; Sun, C.; Huang, G. A chiral elastic metamaterial beam for broadband vibration suppression. *J. Sound Vib.* **2014**, *333*, 2759–2773. [\[CrossRef\]](#)
- Casalotti, A.; El-Borgi, S.; Lacarbonara, W. Metamaterial beam with embedded nonlinear vibration absorbers. *Int. J. Non-Linear Mech.* **2018**, *98*, 32–42. [\[CrossRef\]](#)
- Shuguang, Z.; Tianxin, N.; Xudong, W.; Jialu, F. Studies of band gaps in flexural vibrations of a locally resonant beam with novel multi-oscillator configuration. *J. Vib. Control.* **2015**, *23*, 1663–1674. [\[CrossRef\]](#)

17. Gao, F.; Wu, Z.; Li, F.; Zhang, C. Numerical and experimental analysis of the vibration and band-gap properties of elastic beams with periodically variable cross sections. *Waves Random Complex Media* **2019**, *29*, 299–316. [[CrossRef](#)]
18. Xiao, Y.; Wen, J.; Yu, D.; Wen, X. Flexural wave propagation in beams with periodically attached vibration absorbers: Band-gap behavior and band formation mechanisms. *J. Sound Vib.* **2013**, *332*, 867–893. [[CrossRef](#)]
19. Filippi, M.; Pagani, A.; Carrera, E. High-order finite beam elements for propagation analyses of arbitrary-shaped one-dimensional waveguides. *Mech. Adv. Mater. Struct.* **2020**, 1–9. [[CrossRef](#)]
20. Chen, S.; Song, Y.; Zhang, H. Wave Propagation in L-Shape Beams with Piezoelectric Shunting Arrays. *Shock. Vib.* **2019**, *2019*, 1–14. [[CrossRef](#)]
21. Liu, L.; Hussein, M.I. Wave Motion in Periodic Flexural Beams and Characterization of the Transition between Bragg Scattering and Local Resonance. *J. Appl. Mech.* **2011**, *79*, 011003. [[CrossRef](#)]
22. Liang, X.; Wang, T.; Jiang, X.; Liu, Z.; Ruan, Y.; Deng, Y. A Numerical Method for Flexural Vibration Band Gaps in A Phononic Crystal Beam with Locally Resonant Oscillators. *Crystals* **2019**, *9*, 293. [[CrossRef](#)]
23. Wang, T.; Sheng, M.-P.; Qin, Q.-H. Multi-flexural band gaps in an Euler–Bernoulli beam with lateral local resonators. *Phys. Lett. A* **2016**, *380*, 525–529. [[CrossRef](#)]
24. Li, J.; Li, S. Generating ultra wide low-frequency gap for transverse wave isolation via inertial amplification effects. *Phys. Lett. A* **2018**, *382*, 241–247. [[CrossRef](#)]
25. Wu, X.; Li, Y.; Zuo, S. The study of a locally resonant beam with aperiodic mass distribution. *Appl. Acoust.* **2020**, *165*, 107306. [[CrossRef](#)]
26. Mei, C.; Mace, B.R. Wave Reflection and Transmission in Timoshenko Beams and Wave Analysis of Timoshenko Beam Structures. *J. Vib. Acoust.* **2005**, *127*, 382–394. [[CrossRef](#)]
27. Lv, H.; Zhang, Y. A Wave-Based Vibration Analysis of a Finite Timoshenko Locally Resonant Beam Suspended with Periodic Uncoupled Force-Moment Type Resonators. *Crystals* **2020**, *10*, 1132. [[CrossRef](#)]
28. Leamy, M.J. Exact wave-based Bloch analysis procedure for investigating wave propagation in two-dimensional periodic lattices. *J. Sound Vib.* **2012**, *331*, 1580–1596. [[CrossRef](#)]
29. Lv, H.; Leamy, M.J. Damping Frame Vibrations Using Anechoic Stubs: Analysis Using an Exact Wave-Based Approach. *J. Vib. Acoust.* **2021**, *143*, 1–21. [[CrossRef](#)]
30. Graff, K.F. *Wave Motion in Elastic Solids*; Ohio State University Press: Columbus, OH, USA, 1975.
31. Mei, C. A Wave-Based Analytical Solution to Free Vibrations in a Combined Euler–Bernoulli Beam/Frame and a Two-Degree-of-Freedom Spring–Mass System. *J. Vib. Acoust.* **2018**, *140*, 061001. [[CrossRef](#)]